Modeling the effect of wave-vegetation interaction on wave setup

van Rooijen, Arnold; McCall, RT; van Thiel de Vries, Jaap; van Dongeren, AR; Reniers, Ad; Roelvink, Dano

DOI
10.1002/2015JC011392

Publication date
2016

Document Version
Final published version

Published in
Journal Of Geophysical Research-Oceans

Citation (APA)
van Rooijen, A., McCall, RT., van Thiel de Vries, J., van Dongeren, AR., Reniers, A., & Roelvink, D. (2016). Modeling the effect of wave-vegetation interaction on wave setup. *Journal Of Geophysical Research-Oceans*, *121*(6), 4341-4359. https://doi.org/10.1002/2015JC011392

AGU PUBLICATIONS

JGR

Journal of Geophysical Research: Oceans

RESEARCH ARTICLE

10.1002/2015JC011392

Modeling the effect of wave-vegetation interaction on wave setup

A. A. van Rooijen[1,2], R. T. McCall[1], J. S. M. van Thiel de Vries[3,4], A. R. van Dongeren[1], A. J. H. M. Reniers[1,4], and J. A. Roelvink[1,5]

[1]Department of Applied Morphodynamics, Unit of Marine and Coastal Systems, Deltares, Delft, Netherlands, [2]School of Earth & Environment and UWA Oceans Institute, The University of Western Australia, Crawley, Western Australia, Australia, [3]Hydronamic, Royal Boskalis Westminster NV, Papendrecht, Netherlands, [4]Department of Hydraulic Engineering, Delft University of Technology, Delft, Netherlands, [5]UNESCO-IHE Institute for Water Education, Delft, Netherlands

Key Points:
- Aquatic vegetation controls sea-swell and infragravity wave transformation, and wave setup
- Wave setup is controlled by radiation stresses and mean and nonlinear drag force effects
- Nonlinear wave-vegetation effects can be simulated using an empirical wave shape model

Correspondence to:
A. A. van Rooijen,
arnold.vanrooijen@deltares.nl

Citation:
van Rooijen, A. A., R. T. McCall, J. S. M. van Thiel de Vries, A. R. van Dongeren, A. J. H. M. Reniers, and J. A. Roelvink (2016), Modeling the effect of wave-vegetation interaction on wave setup, *J. Geophys. Res. Oceans*, *121*, 4341–4359, doi:10.1002/2015JC011392.

Received 10 OCT 2015
Accepted 16 MAY 2016
Accepted article online 19 MAY 2016
Published online 25 JUN 2016

Abstract Aquatic vegetation in the coastal zone attenuates wave energy and reduces the risk of coastal hazards, e.g., flooding. Besides the attenuation of sea-swell waves, vegetation may also affect infragravity-band (IG) waves and wave setup. To date, knowledge on the effect of vegetation on IG waves and wave setup is lacking, while they are potentially important parameters for coastal risk assessment. In this study, the storm impact model XBeach is extended with formulations for attenuation of sea-swell and IG waves, and wave setup effects in two modes: the sea-swell wave phase-resolving (nonhydrostatic) and the phase-averaged (surfbeat) mode. In surfbeat mode, a wave shape model is implemented to capture the effect of nonlinear wave-vegetation interaction processes on wave setup. Both modeling modes are verified using data from two flume experiments with mimic vegetation and show good skill in computing the sea-swell and IG wave transformation, and wave setup. In surfbeat mode, the wave setup prediction greatly improves when using the wave shape model, while in nonhydrostatic mode (nonlinear) intrawave effects are directly accounted for. Subsequently, the model is used for a range of coastal geomorphological configurations by varying bed slope and vegetation extent. The results indicate that the effect of wave-vegetation interaction on wave setup may be relevant for a range of typical coastal geomorphological configurations (e.g., relatively steep to gentle slope coasts fronted by vegetation).

1. Introduction

Aquatic vegetation (e.g., kelp, mangroves, marshes, and seagrass) in the coastal zone attenuates wave energy, reduces current magnitudes, and decreases wave runup and overtopping [e.g., *Dalrymple et al.*, 1984; *Kobayashi et al.*, 1993; *Dubi*, 1995; *Løvås*, 2000; *Quartel et al.*, 2007; *Horstman et al.*, 2014; *Möller et al.*, 2014]. As a result of this mitigating effect on coastal hazards, vegetation can reduce costs for coastal protection. On many of the world's shorelines, vegetation is already implicitly part of the flood defense system, and coastal managers and engineers are becoming increasingly aware of its important safety function [e.g., *Mazda et al.*, 1997; *Koch et al.*, 2009; *Borsje et al.*, 2011]. In order to take advantage of this function, the effect of vegetation needs to be quantified so that natural coastal protection measures, so-called nature-based flood defenses, can be designed.

To date, the best-known effect of vegetation in the nearshore zone is the attenuation of (wind-generated) sea-swell waves [e.g., *Mendez and Losada*, 2004]. Recently, two additional effects have been identified. First, *Dean and Bender* [2006] found that the presence of vegetation may lead to a reduction of wave setup or even set-down, in case of emergent vegetation and/or nonlinear (skewed) waves. The findings of *Dean and Bender* [2006] were confirmed by *Wu et al.* [2011], who carried out wave flume experiments on a flat and sloping bottom with and without vegetation. Although this effect of vegetation has been acknowledged by several authors [e.g., *Lövstedt and Larson*, 2010; *Stratigaki et al.*, 2011; *Akgul et al.*, 2013], only a limited number of studies aimed to quantify these effects [e.g., *Ma et al.*, 2013; *Guannel et al.*, 2015], and thus the effect of vegetation on the mean water level through wave setup is often ignored in flood risk assessments.

Second, infragravity (IG) waves have been identified as an important driver for wave runup [e.g., *Ruggiero et al.*, 2001; *Stockdon et al.*, 2006] and dune erosion on sandy shores [e.g., *van Thiel de Vries*, 2009]. However,

relatively little is known about IG motions in the presence of vegetation. *Phan et al*. [2015] studied the relative importance of IG waves in presence of mangrove trees and found through numerical simulations that they become dominant over sea-swell waves after a certain propagation distance. In particular, they found that IG waves require relatively long distances to dissipate and hypothesized that they play an important role in providing the hydrodynamic conditions for a healthy mangrove ecosystem.

In recent years, several numerical models have been developed or extended to include wave attenuation by vegetation. These models can be generally divided into (sea-swell wave) phase-resolving [e.g., *Ma et al*., 2013; *Wei and Jia*, 2014; *Tang et al*., 2015] and phase-averaged models [e.g., *Suzuki et al*., 2012; *Phan et al*., 2015]. Phase-resolving (e.g., Boussinesq type and nonhydrostatic) models resolve the entire wave spectrum, including nonlinear sea-swell motions, and (the generation of) IG waves. Phase-averaged models (e.g., SWAN and XBeach-surfbeat), on the other hand, do not resolve the phase of the sea-swell waves and use parameterizations instead, usually based on linear wave theory. The advantage of these latter models is that they are computationally much cheaper and are more applicable for engineering purposes (e.g., SWAN) [see *Suzuki et al*., 2012]. Recently, *Guannel et al*. [2015] presented a 2DV integrated modeling framework for erosion of sandy and muddy coasts fronted by vegetation using widely applied empirical concepts and a relatively simple modeling approach, as well as new formulations for the effect of vegetation on wave setup based on the work of *Dean and Bender* [2006]. Note that most existing models are based on a concept where vegetation is schematized as rigid cylinders, even though they are commonly applied to a range of vegetation types including flexible vegetation (e.g., seagrass). Novel methods in which the plant flexibility and motion due to flow can be accounted for have been developed in recent years [*Abdelrhman*, 2007; *Dijkstra and Uittenbogaard*, 2010; *Mullarney and Henderson*, 2010]. Currently, the use of these kind of models for wave-dominated conditions is still in an experimental stage [e.g., *Döbken*, 2015].

In this paper, we extend the XBeach model [*Roelvink et al*., 2009] to provide a process-based tool to assess vegetation effects on sea-swell and IG waves, and wave setup. This model can be run in phase-resolving ("nonhydrostatic") and phase-averaged ("surfbeat") mode. For both modes, formulations are implemented to take into account vegetation-induced sea-swell wave attenuation, IG wave attenuation, mean flow reduction, and mean water level effects assuming schematized (rigid) vegetation. Both modes capture the essential physics of the vegetation effects on waves and wave setup, and are validated by means of comparison with data collected in two flume experiments with mimic vegetation. Subsequently, the model is used to study the sensitivity of wave setup reduction by vegetation to variation in the location of vegetation along the cross-shore bottom profile and the profile slope itself. While the model is strictly not derived and verified for natural vegetation, it does provide a first indication of the relevance of these specific vegetation processes on varying coastal geomorphological settings.

2. The Effect of Vegetation on Wave Setup

Waves propagating through a vegetation field exert a drag force on the plants. Ignoring plant swaying motion and inertial forces, the resulting vegetation force acting on the water column (F_D) is given by [*Morison et al*., 1950; *Dalrymple et al*., 1984]:

$$F_D = \frac{1}{2}\rho C_D b_v N_v u|u| \tag{1}$$

where ρ is the water density, C_D is the drag coefficient, b_v is the vegetation stem width, N_v is the vegetation density, and u is the horizontal (wave-induced) velocity. When applied to linear wave theory, the work done by the vegetation drag force on the water column can be used to compute wave energy loss [e.g., *Mendez and Losada*, 2004].

This effect of vegetation on incident wave energy is well established but—as stated in the introduction—effects on wave setup and IG waves are not well established yet. Assuming linear waves and fully submerged vegetation, integration of equation (1) over a wave period leads to zero net force on the water column, and hence has no direct effect on wave setup. However, four different mechanisms by which vegetation may affect the wave setup have been identified in literature:

1. Change of the cross-shore radiation stress gradient profile [e.g., *Longuet-Higgins and Stewart*, 1964; *Buckley et al*., 2016];

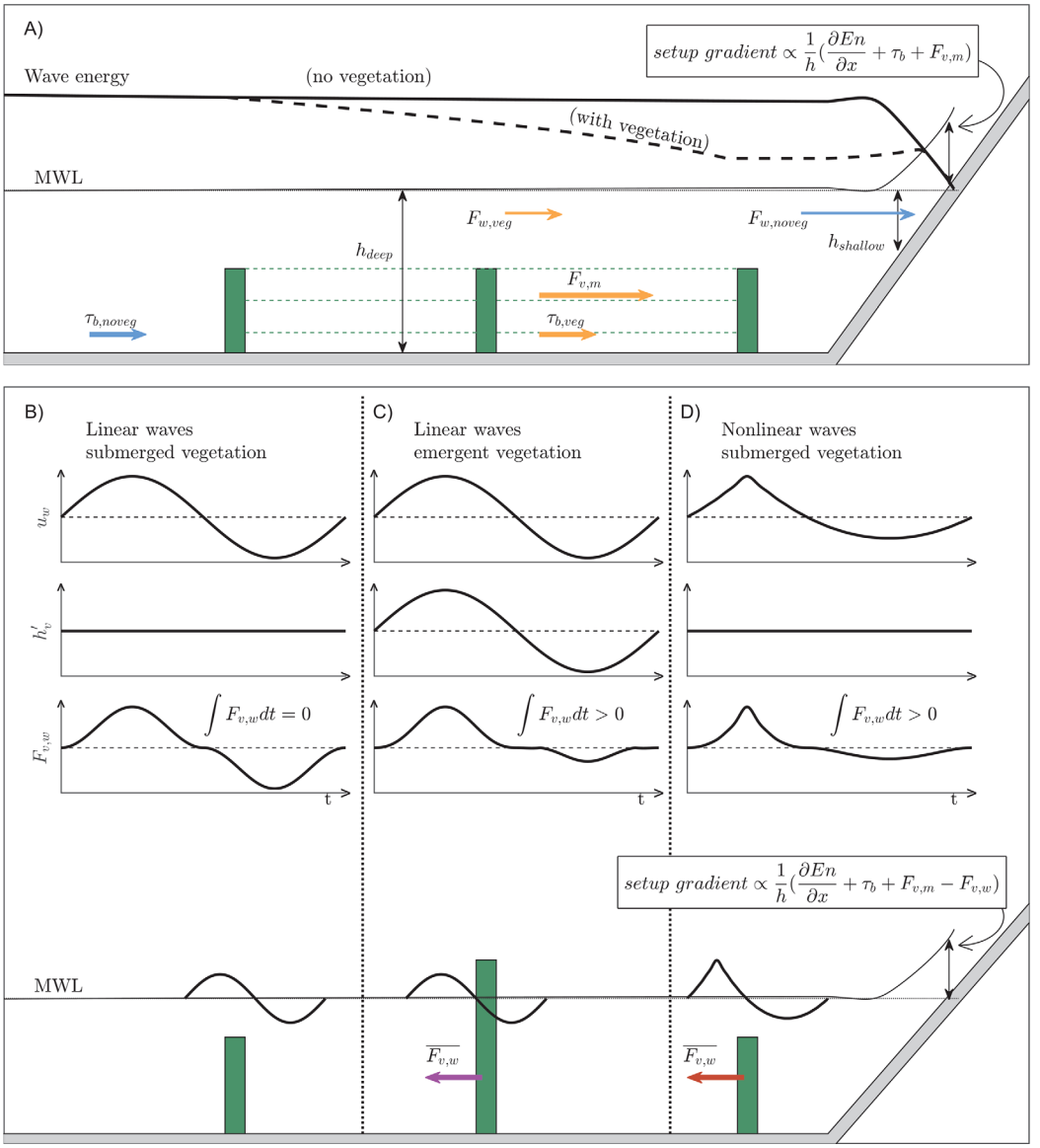

Figure 1. Definition sketch of wave-vegetation interaction (represented by cylindrical elements) and the resulting wave-averaged net forces and shear stress (τ_b) acting on the water column, and the effect on the wave setup or mean water level. All forces and bed shear stresses are shown as they act on the water column. (a) The presence of rigid elements results in radiation stress gradients in relatively deep water, resulting in a reduced wave force (F_w), and mean vegetation force ($F_{v,m}$) due to the mean flow (i.e., undertow) drag. Schematic intrawave velocity time trace (u_w), submerged vegetation height (h'_v), and resulting intrawave vegetation force ($F_{v,w}$) for linear waves in combination with (b) submerged and (c) emergent vegetation, and (d) nonlinear waves in combination with submerged vegetation. For all three cases, the net resulting vegetation force acting on the water column ($F_{v,w}$) is indicated by the colored arrows (where the overbar indicates integration over time).

2. Mean drag force due to mean flow, e.g., undertow (often represented as change in the magnitude of bed shear stresses) [e.g., *Svendsen*, 2006; *Løvås and Tørum*, 2001; *Luhar et al.*, 2010];
3. Variation of the submerged vegetation height over a wave period in case of emergent vegetation, resulting in a net wave-averaged drag force [*Dean and Bender*, 2006];
4. Nonlinear intrawave drag force that is exerted on the vegetation stems in case of nonlinear (skewed) waves, resulting in a net wave-averaged drag force [*Dean and Bender*, 2006].

The strength of these mechanisms and their relative importance depend on the local geometry (e.g., bed slope and water depth), vegetation characteristics (e.g., density, height, and location), and wave conditions. All four mechanisms are visualized in Figure 1, and are discussed in more detail below.

2.1. Radiation Stress Gradients

As waves propagate toward the coast conservation of energy flux results in a local increase in wave energy (shoaling) followed by a relatively strong decrease (dissipation) due to breaking. The result of this variation is a nonzero wave-induced radiation stress gradient which—divided by local water depth—is a horizontal force (F_w) that acts on the water column. In the absence of vegetation, the radiation stress gradient (Figure 1a, blue arrow, $F_{w,noveg}$) is balanced by the bed shear stress and a pressure gradient (i.e., wave setup). In case of wave energy dissipation due to vegetation (Figure 1a, black dashed line), radiation stress gradients become greater in relatively deep water and smaller in shallow water. This results in a smaller wave force acting on the water column (Figure 1a, orange arrow $F_{w,veg}$), leading to reduced wave setup [e.g., *Buckley et al*., 2016].

2.2. Mean Drag Force

The presence of aquatic vegetation has an effect on mean flows such as the undertow. This is often taken into account through the bed shear stress, which is usually computed as a function of the quadratic velocity and a friction coefficient [e.g., *Ruessink et al*., 2001]. Here we represent this effect as a mean drag force on the stems, which has a similar form (Figure 1a, orange arrow, $F_{v,m}$). The mean near-bed current is directed offshore, resulting in a net mean drag force acting on the stems, which causes an onshore-directed reaction force acting on the water column ($F_{v,m}$). Hence, contrary to the effect of the change of the cross-shore gradient in radiation stress, the wave setup is expected to increase due to the increase in the mean drag force (or bed shear stress cf. *Apotsos et al*. [2007]). This effect has previously been observed by, e.g., *Løvås and Tørum* [2001] and *Luhar et al*., [2010].

For clarity, the bed shear stress (τ_b) is also depicted for the case without and with vegetation (Figure 1a, respectively, blue and orange arrow). However, since the mean drag effect is not incorporated in the bed shear stress, this is considered here mainly a function of the actual bed roughness, and not the vegetation.

2.3. Wave-Induced Force Due to Emergent Vegetation

When applying linear wave theory to submerged vegetation and integrating the vegetation drag force over a wave cycle, the net resulting force due to momentum loss equals zero. However, *Dean and Bender* [2006] showed that for emergent vegetation, the net force is nonzero. This is a result of the variation of the local water depth over a wave cycle, due to which a larger part of the vegetation stem interacts with the water column under the wave crest than under the trough. For clarity, we use the term "submerged vegetation height" here to distinguish the total vegetation height that is submerged and exposed to flow. In case of fully submerged vegetation, the submerged vegetation height is equal to the height of the plants. In case of fully emergent vegetation (i.e., vegetation top is above wave crest level), the submerged vegetation height is equal to the instantaneous water depth, which varies between wave crest and trough level within the wave cycle. Finally, in case of partly emergent vegetation (i.e., the vegetation top is in between the wave crest and trough), the submerged vegetation height is the minimum of the plant height and the local water depth. In Figures 1b and 1c, this effect is schematically visualized by means of time trace of the wave orbital velocity (u_w), the submerged vegetation height (h'_v), and the resulting vegetation force ($F_{v,w}$). For clarity, we assume depth-averaged orbital velocities and vertically uniform vegetation. The depth-integrated vegetation force is then proportional to:

$$F_{v,w} \propto u_w|u_w| \cdot h'_v \tag{2}$$

In case of linear waves in combination with submerged vegetation, the net force (integrated over one wave period) is zero (Figure 1b). In case of linear waves in combination with emergent vegetation, the submerged vegetation height varies over a wave cycle; a larger part of the vegetation is submerged under the wave crest than under the wave trough (Figure 1c). The vegetation force integrated over a wave cycle is nonzero and acts opposite to the direction of wave propagation on the water column (Figure 1c, purple arrow), balancing the radiation stress gradient in part and decreasing wave setup [*Dean and Bender*, 2006]. It should be noted that the model employed in this study does not account for variations in the submerged vegetation height due to the bending of flexible vegetation.

2.4. Wave-Induced Force Due to Skewed Waves

Dean and Bender [2006] found a similar effect in case of nonlinear, skewed waves, even for fully submerged vegetation (Figure 1d). For skewed waves, the depth-averaged velocity profile over one wave period shows a relatively sharp peak in the direction of wave propagation, and a relatively flat trough. Due to the quadratic relation in the drag force formulation (equation (1)), the resulting drag force profile over a wave cycle is asymmetrical. After integrating over a wave period, a net force is found that acts against the direction of wave propagation on the water column (Figure 1d, red arrow). Again, this results in reduction of the wave setup [*Dean and Bender*, 2006].

3. Methods

XBeach [*Roelvink et al*., 2009] was originally developed as a phase-averaged model that resolves amplitude variation on the wave group scale of sea-swell waves (surfbeat), but does not resolve their phase. The amplitude variation in time and space drives lower frequency infragravity-band (IG) motions, which are resolved using the nonlinear shallow water equations (NLSWE). The model includes sediment transport and morphological changes and has successfully been applied to model dune erosion, overwash, and breaching processes on sandy beaches during extreme events [e.g., *Roelvink et al*., 2009; *van Thiel de Vries*, 2009; *McCall et al*., 2010], and, more recently, to study coral reef hydrodynamics [e.g., *Van Dongeren et al*., 2013; *Quataert et al*., 2015]. Recently, a nonhydrostatic mode was developed for XBeach [*Smit et al*., 2010; *McCall et al*, 2014], which is similar to (in fact, a prototype of) a depth-averaged version of the SWASH model [*Zijlema et al*., 2011; *Smit et al*., 2013] and is able to fully resolve sea-swell waves.

In the current study, both the surfbeat and nonhydrostatic mode of XBeach are extended to include the effect of vegetation on sea-swell waves, IG waves, and mean flow. In the following, both XBeach modes are described separately. For clarity, we will refer to the *surfbeat* and *nonhydrostatic* mode throughout the paper for the phase-averaged (hydrostatic) and phase-resolving modes, respectively. Although all model formulations were implemented in 2DH, this study focuses on wave propagation in cross-shore direction. For clarity, all model formulations are therefore written in their 1-D equivalent. Default model settings are used in all simulations (XBeach version v1.21.4682), unless reported otherwise. Since the nonhydrostatic model formulations include more physics, we will initially discuss the nonhydrostatic mode (section 3.1). Subsequently, the implementation of vegetation effects in the surfbeat mode of XBeach is presented (section 3.2).

3.1. Nonhydrostatic Mode

The governing equations for the nonhydrostatic mode are based on the (depth-averaged) NLSWE extended with a nonhydrostatic pressure term following *Stelling and Zijlema* [2003]:

$$\begin{gathered}\frac{\partial \eta}{\partial t}+\frac{\partial uh}{\partial x}=0\\ \frac{\partial u}{\partial t}+u\frac{\partial u}{\partial x}-\upsilon_h\frac{\partial^2 u}{\partial x^2}=-g\frac{\partial \eta}{\partial x}-\frac{\partial \overline{q}}{\partial x}-\frac{\tau_{b,x}}{\rho h}+\frac{F_{v,nh}}{\rho h}\end{gathered} \tag{3}$$

where x and t are the horizontal and temporal coordinates, respectively, η is the water surface elevation, u is the depth-averaged velocity, h is the local water depth, υ_h is the horizontal viscosity, g is the gravitational constant, $\overline{q}$ is the depth-averaged dynamic pressure, $\tau_{b,x}$ is the bed shear stress (following *Ruessink et al*. [2001]), and $F_{v,nh}$ is the vegetation force. For a more in-depth model description of XBeach nonhydrostatic mode, reference is made to *Smit et al*. [2010] and *McCall et al*. [2014].

The depth-averaged vegetation force ($F_{v,\mathrm{nh}}$) is equal to the drag force (F_D, equation (1)) integrated over the vegetation height, where u is the depth-averaged velocity due to the combination of mean flow, IG waves and sea-swell wave orbital motion. This approach is similar to *Ma et al*. [2013] and *Wei and Jia* [2014]. Note that the vegetation effects are incorporated in the vegetation force only and not in the bed shear stress (i.e., we use a constant friction coefficient). Using this set of equations, the effects of emergent vegetation and nonlinear waves (section 2) are included directly.

3.2. Surfbeat Mode

3.2.1. Sea-Swell Wave Propagation

XBeach surfbeat mode solves the time-dependent sea-swell wave action (sea-swell wave amplitude) on the scale of wave groups, which drives steady and unsteady (IG) motions through radiation stress gradients in the NLSWE. The sea-swell wave action balance is given by [e.g., *Phillips*, 1977]:

$$\frac{\partial A}{\partial t}+\frac{\partial c_{g,x}A}{\partial x}=-\frac{D_w+D_v}{\sigma} \tag{4}$$

where $A=E_w/\sigma$, E_w is the (sea-swell) wave energy, σ is the intrinsic wave frequency, and c_g is the wave group velocity. Sea-swell wave energy dissipation due to breaking (D_w) is computed using *Roelvink* [1993]. The formulation by *Mendez and Losada* [2004] is used for wave dissipation due to vegetation (D_v):

$$D_v=\left(\frac{kg}{2\sigma}\right)^3\frac{\rho C_D b_v N_v}{2\sqrt{\pi}}\frac{\sinh^3 kh_v+3\sinh kh_v}{3k\cosh^3 kh}{H_{rms}}^3 \tag{5}$$

where k is the wave number, C_D is a (bulk) drag coefficient, H_{rms} the root-mean-square wave height ($=\sqrt{8\cdot E_w/(\rho g)}$), and h_v the vegetation height which is limited to the local water depth (h) in case of emergent vegetation. The approximation by *Mendez and Losada* [2004] is commonly used to compute wave energy dissipation by vegetation and has been incorporated in several models [e.g., *Suzuki et al*., 2012; *Guannel et al*., 2015].

3.2.2. IG Waves and Mean Flow

Steady (mean setup, undertow, and longshore currents) and unsteady water motions (IG waves) on the time scale of wave groups are solved using the (depth-averaged) NLSWE:

$$\begin{aligned}\frac{\partial \eta}{\partial t}+\frac{\partial u^L h}{\partial x}&=0\\ \frac{\partial u^L}{\partial t}+u^L\frac{\partial u^L}{\partial x}&=-g\frac{\partial \eta}{\partial x}-\frac{\tau_{b,x}+F_w+F_v}{\rho h}\end{aligned} \tag{6}$$

where η is the water surface elevation, u^L is the depth-averaged Lagrangian velocity, $\tau_{b,x}$ is the bed shear stress (following *Ruessink et al*. [2001]), F_w is the (radiation stress) wave force, and F_v is the wave-averaged vegetation force. Since here the mean drag is not incorporated in the bed shear stress (i.e., we use a constant friction coefficient), only the wave force and vegetation force are directly influenced by the presence of vegetation in the water column (see section 2). This is explained further in the next section.

3.2.3. Vegetation Mechanisms Affecting the Mean Water Level or Wave Setup

The radiation-stress-induced wave force (F_w) is computed using the wave and roller energy obtained from the sea-swell wave action balance (equation (4)) and the roller energy balance (not shown here), respectively [*Reniers et al*., 2004; *Roelvink et al*., 2009]. The vegetation force (F_v) acting on the water column can be divided into a component related to the sea-swell wave orbital motion scale and a component related to sea-swell wave phase-averaged (or: mean) time scale [e.g., *Zhou and Graham*, 2000]:

$$F_v=F_{v,m}+F_{v,w} \tag{7}$$

where $F_{v,m}$ is the vegetation force component related to mean (e.g., undertow) and unsteady (e.g., IG waves) currents [*Svendsen*, 2006], and $F_{v,w}$ is the component related to effects on the sea-swell wave orbital motion scale [*Dean and Bender*, 2006].

3.2.3.1. Vegetation Force Component Related to Mean and IG Flow

The component of the vegetation force associated with the mean and IG-wave flow ($F_{v,m}$) is computed using the Eulerian velocity (u^E) [see *Roelvink et al*., 2009] in combination with equation (1). It is appropriate to include the IG waves within the vegetation force component related to mean flow in this manner since the IG wave orbital excursion is generally much larger than the spacing between vegetation stems and can therefore be considered as unsteady currents [*Svendsen*, 2006].

3.2.3.2. Vegetation Force Component Related to Sea-Swell Orbital Motion

Since the model in surfbeat mode does not compute the incident wave phase, we adopted a modeling approach similar to the wave shape model of *van Thiel de Vries* [2009] to account for the effects of nonlinear sea-swell waves and/or emergent vegetation (as explained in section 2), and to compute the resulting component of the vegetation force ($F_{v,w}$). The model utilizes the wave shape description of *Rienecker and Fenton* [1981]

and an empirical relation by *Ruessink et al*. [2012] to compute a time series of the depth-averaged orbital velocity and water surface elevation over one wave cycle. A more detailed description of the wave shape model is provided in Appendix A.

Using these time series, the net resulting component of the vegetation force associated with sea-swell wave orbital motions ($F_{v,w}$) is computed at every (vegetated) model grid point by integrating the intrawave vegetation force over one wave cycle:

$$F_{v,w} = \int_0^{T_{rep}} \frac{1}{2} \rho C_D b_v N_v u_w |u_w| dt \tag{8}$$

where T_{rep} is the representative wave period, typically the $T_{m\text{-}1,0}$ spectral wave period. In case of emergent vegetation, the intrawave surface elevation time series is used to estimate the submerged vegetation height (h'_v) in equation (2).

Note that the wave shape model is based on empirical relations valid for nonvegetated beaches. The results of *Wu et al*. [2011] suggest that waves become less asymmetric but more skewed in presence of vegetation compared to the situation without vegetation. As a consequence, the effect of nonlinear waves on the wave setup may generally be even greater than assumed here. However, to the authors' knowledge, no literature exists that quantifies the effect of vegetation on the wave shape. We further assume a uniform (bulk) drag coefficient C_D for sea-swell (in the wave action balance, and for the short-wave-induced net vegetation force), IG waves and mean flow (within the NLSWE), which is consistent with previous studies [*Zhou and Graham*, 2000; *Luhar et al*., 2010; *Guannel et al*., 2015].

4. Results

The performance of XBeach in both modes is evaluated using two laboratory data sets with mimic vegetation. Although the methodology used for sea-swell wave energy attenuation (equation (5)) has been validated extensively in literature, here the formulations were implemented in an instationary wave model, including infragravity (IG) waves. Therefore, the model is first verified for both sea-swell and IG wave attenuation using the flume experiments by *Løvås* [2000] [cf. *Mendez and Losada*, 2004; *Suzuki et al*., 2012; *Ma et al*., 2013]. Subsequently, the data set of *Wu et al*. [2011] is used to verify the model for vegetation effects on wave setup. Finally, the importance of the effect of vegetation on wave setup on different coastal geomorphological configurations is investigated by varying the bed slope and vegetation configuration.

4.1. Sea-Swell and Infragravity Wave Attenuation

Løvås [2000] and *Løvås and Tørum* [2001] studied the effect of kelp vegetation on wave propagation, runup, and dune erosion using flume experiments with waves propagating over artificial kelp (*L. hyperborea*) vegetation. The experiments were carried out in a 40 m long wave flume at SINTEF, Norway. A sandy cross-shore profile was applied with a surf zone slope of 1/30, and several runs were carried out with and without vegetation (Figure 2m). The fully submerged model vegetation had an effective height of about 0.09 m and was placed at about 0.3–0.5 m water depth. The number of plants per unit area was $N_v = 1200$ units/m^2. The test program included random wave simulations with two peak wave periods (2.5 and 3.5 s) and two wave heights. Additionally, two experiments were carried out in which the water depth was lowered, resulting in a total of six different experiments. Note that the wave maker that was used in the experiments was not equipped with an active reflection compensation system to dampen reflected (IG) waves [*Løvås and Tørum*, 2001].

XBeach is set up in nonhydrostatic and surfbeat mode using the flume dimensions and vegetation characteristics as discussed above. The (bulk) drag coefficient C_D is estimated as function of the Keulegan-Carpenter number ($KC = u_c T_p / b_v$, where u_c is a characteristic velocity acting on the plant) using the relation by *Mendez and Losada* [2004] that was derived specifically for the kelp mimics that were used in these experiments. Given the relatively complex shape of the kelp mimics [*Løvås and Tørum*, 2001] and the resulting uncertainty in determining the correct plant diameter (b_v), as well as the fact that the computed C_D-values were all close to 0.2 (0.13–0.27), we apply a constant bulk drag coefficient of 0.2 in all simulations. At the offshore boundary, a JONSWAP spectrum with peak enhancement factor $\gamma_{jsp} = 7.0$ is applied, equal to

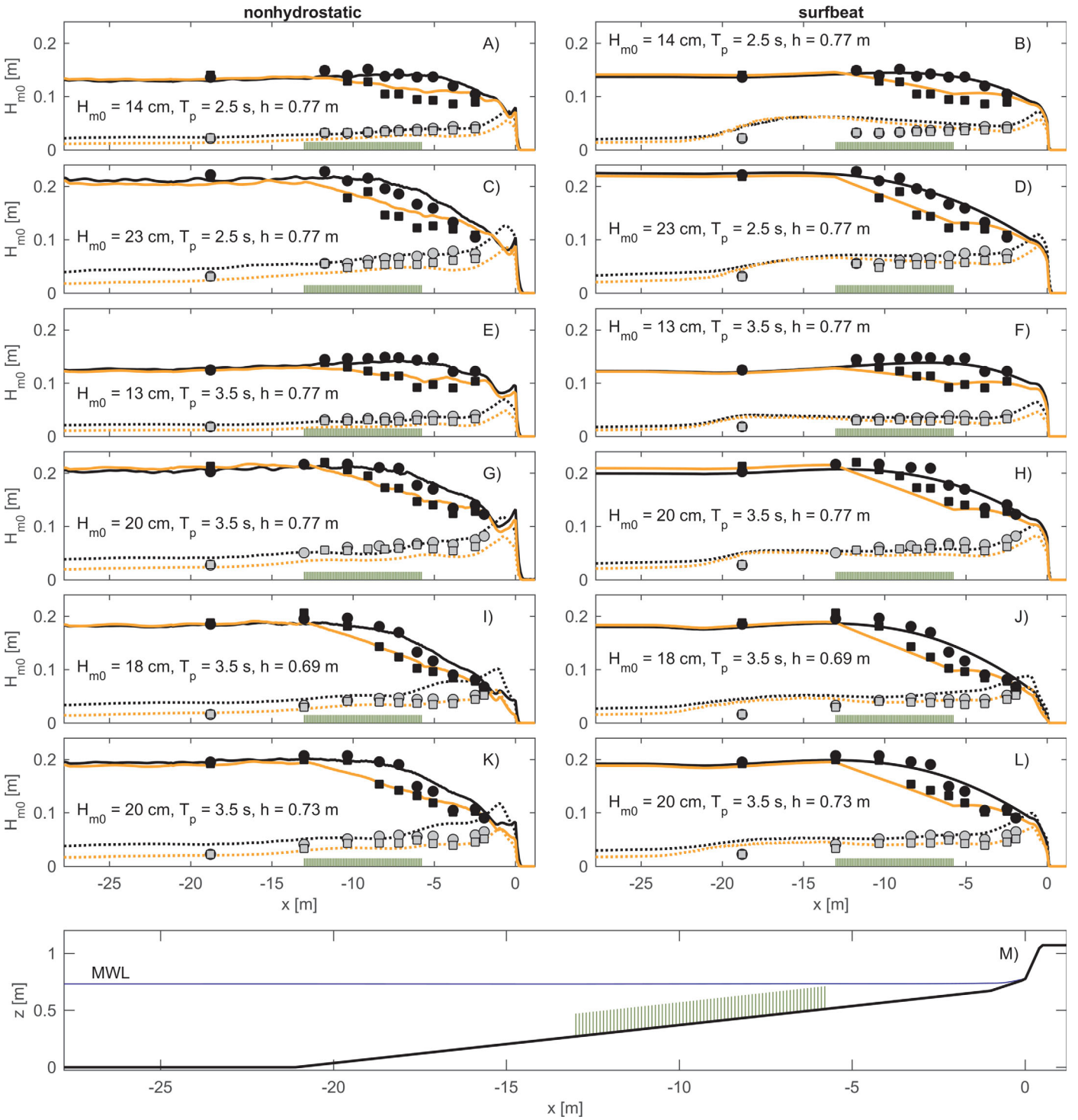

Figure 2. Model-data wave height comparison for (a, c, e, g, i, k) XBeach nonhydrostatic and (b, d, f, h, j, l) surfbeat mode using the experimental data of *Løvås* [2000]. Sea-swell (model: solid line, measurements: black symbols) and infragravity (model: dotted line, measurements: grey symbols) wave heights are shown for six different experiments (corresponding hydraulic conditions are indicated in the plots) without vegetation (model: black line, measurements: circles) and with vegetation (model: orange line, measurements: squares) present on the beach slope. The experimental setup including the location of the vegetation patch is shown in Figure 2m.

the value used during the experiments [*Løvås*, 2000]. In order to reproduce the experiments as best possible, the active reflection compensation routine in XBeach is turned off for these cases and first-order wave steering was applied as in the physical model tests. Hence, all IG waves are generated inside the model

Table 1. XBeach Model Skill for the *Løvås* [2000] Cases[a]

	Nonhydrostatic No Vegetation	Nonhydrostatic With Vegetation	Surfbeat No Vegetation	Surfbeat With Vegetation
SS waves SCI	0.08	0.09	0.07	0.09
SS waves BIAS (cm)	0.33	0.29	0.06	−0.31
IG waves SCI	0.25	0.24	0.26	0.24
IG waves BIAS (cm)	0.55	−0.86	0.79	0.32

[a]Values represent scatter index (SCI) and bias for sea-swell (SS) and infragravity (IG) waves. A positive bias indicates overprediction by the model.

domain rather than at the offshore boundary of the model. All other model settings such as the wave breaking parameters are kept default for both modes.

In the following, the sea-swell and IG wave transformation are considered separately. The measurement data and model results are separated into a sea-swell and IG component assuming a split frequency that equals half the wave peak frequency (i.e., for the cases with $T_p = 2.5$ s, $f_{split} = 0.2$ Hz; for $T_p = 3.5$ s, $f_{split} = 0.14$ Hz). The model results are quantified through calculation of the bias and scatter index (SCI) as proposed for wave models by *Van der Westhuysen* [2010].

4.1.1. Nonhydrostatic Mode

The nonhydrostatic mode (Figures 2a, 2c, 2e, 2g, 2i, and 2k) is able to accurately capture the sea-swell wave evolution in case of a plane beach as well as with vegetation present. In the breaker zone, wave heights are slightly overestimated (bias = 1.1 cm, SCI = 0.12), while in the vegetation zone, the wave attenuation shown by the measurements is accurately (bias = 0.09 cm, SCI = 0.07) reproduced by the model. Since during the experiments and in the model first-order wave steering was applied at the boundary, all IG waves are generated within the flume/model domain itself. In general, the model is able to compute the generation reasonably well. The IG waves are overestimated for the two cases with an altered water depth (Figures 2i and 2k), particularly in the breaker zone (bias = 1.2 cm, SCI = 0.39). The data show that the effect of vegetation on IG waves is relatively limited in these cases. The reduction in IG wave energy due to vegetation was in the order of a few percent, which falls within the experimental uncertainty range. In the model, the effect of the vegetation on the IG wave height is somewhat overestimated. However, overall a good match is found between model results and measurements (i.e., a limited effect of the presence of vegetation on IG wave generation and propagation).

The overall model skill is determined by computing the SCI and bias for the sea-swell wave height and the IG wave height based on all cases and measurement locations (Table 1). The SCI and bias are considered accurate and indicate the model is able to predict both sea-swell and IG wave transformation without requiring a detailed calibration.

4.1.2. Surfbeat Mode

In surfbeat mode, the sea-swell wave height is accurately captured (Figures 2b, 2d, 2f, 2h, 2j, and 2l), both with and without vegetation present (bias = −0.12 cm, SCI = 0.08). The results are similar to *Mendez and Losada* [2004], and indicate that their approximation is also applicable for instationary, surfbeat-type models. The IG wave height transformation is reasonably well represented by the model (bias = −0.15 cm, SCI = 0.26), and the limited effect of the vegetation on these waves (average IG wave energy reduction of 2%) is better reproduced (4%) compared to the nonhydrostatic mode (15%). Note that due to the limited water depth (0.3–0.5 m) at the vegetation patch, waves are close to breaking and may be highly asymmetric and nonlinear. This effect is explicitly taken into account in nonhydrostatic but not in surfbeat mode (which is based on linear wave theory). Nevertheless, the wave propagation is accurately captured for both modes (Figure 2), hence wave nonlinearity does not seem to have a significant effect here.

The overall model skill is determined by computing the SCI and bias for all cases and measurement locations (Table 1), and shows similar values compared to the nonhydrostatic mode. These results indicate that the surfbeat mode is also able to predict both sea-swell and IG wave heights without requiring a detailed calibration.

4.2. Wave Setup Effects

Wu et al. [2011] carried out an extensive study to investigate surge and wave reduction by vegetation. The research project included laboratory and field experiments as well as numerical modeling. As part of this project, *Ozeren et al*. [2014] reported on experiments for both rigid and flexible model vegetation, as well as live vegetation over a horizontal bed.

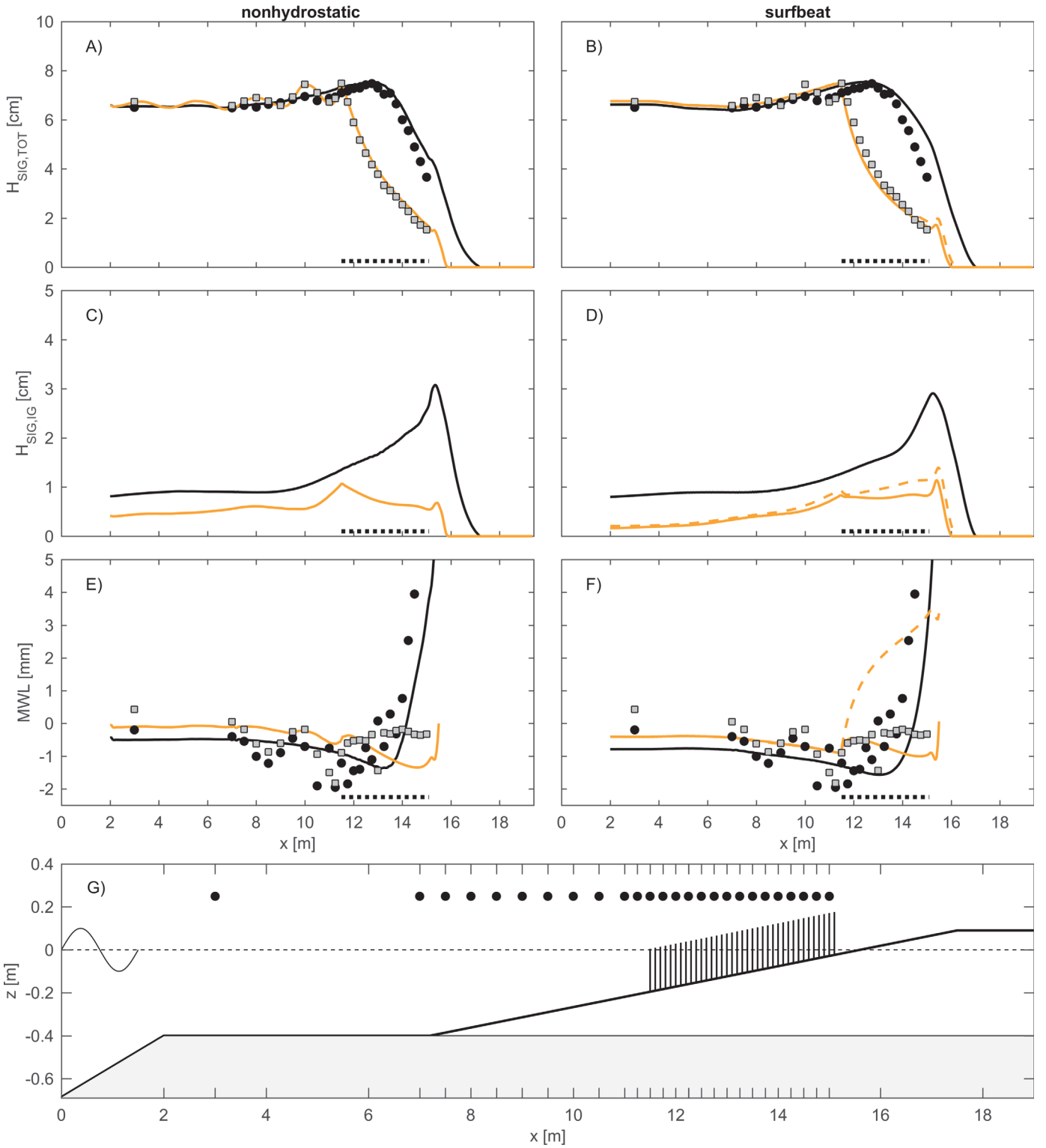

Figure 3. (a, b) Significant (total) wave height, (c, d) infragravity wave height, and (e, f) mean water level computed with (a, c, e) XBeach nonhydrostatic and (b, d, f) surfbeat mode without (black) and with vegetation (orange) and using surfbeat mode without wave shape model (orange dashed) for experiment r40091240 reported by *Wu et al.* [2011]. Measurements are indicated with the black and grey symbols (respectively, without and with vegetation). Note that the measurements shown in Figures 3b and 3f are identical to Figures 3a and 3e, respectively, and are repeated for model-data comparison. (g) Experimental setup for the flume experiments [*Wu et al.*, 2011], including the 1:21 beach profile (white), false flume bottom (grey), and the model vegetation patch (black). The still water level is represented by the dashed line. Wave gauge positions are indicated by the dots and the *x* axis ticks.

Table 2. Model Forcing Conditions for the *Wu et al.* [2011] Cases

Reference ID	H_s (m)	T_p (s)	L_p (m)	H_s/L_p	ξ
r40039120	0.037	1.2	1.936	0.019	0.35
r40057160	0.047	1.6	2.836	0.017	0.37
r40058120	0.054	1.2	1.936	0.028	0.28
r40065180	0.055	1.8	3.269	0.017	0.37
r40085160	0.074	1.6	2.836	0.026	0.30
r40091240	0.067	2.4	4.532	0.015	0.39
r40098180	0.079	1.8	3.269	0.024	0.31

For this study, the flume experiments with irregular waves and vegetation on a sloping bed as described by *Wu et al.* [2011] are particularly relevant. The experiments were carried out in a 20.6 m long, 0.69 m wide, 1.22 m deep wave flume at the National Sedimentation Laboratory of the United States Department of Agriculture. The bottom profile used in the experiments consisted of a 0.29 m high false floor of plywood with on top a plane wooden beach with a 1:21 slope (Figure 3g). The toe of the beach was located at x = 7.2 m. To guarantee a gradual wave transition, a 1:7 slope was built in front of the false floor. The vegetation was represented by 20 cm high (0.6 m full scale), 3.2 mm diameter (9.6 mm full scale) birch dowels and were organized in a staggered pattern with an equal spacing of 19.1 mm. The vegetation patch was positioned between x = 11.5 m and x = 15.1 m with a density of 3182 units/m^2 (representing a full-scale density of 350 units/m^2). The water surface elevation was measured using five capacitance-type wave probes with a sampling rate of 30 Hz. One wave gauge was located at x = 3 m, and experiments were repeated with different wave gauge positions to increase the spatial resolution of the wave data resulting in a maximum resolution of 0.25 m between x = 11 m and x = 15 m (Figure 3g). The experimental program included both regular and irregular wave experiments. For this study, the results obtained with irregular waves and rigid vegetation are particularly relevant and were used. Each irregular wave experiment was conducted with and without vegetation for the duration of 100 times T_p and was repeated five times (each time with an identical JONSWAP-spectrum but a different irregular signal). The hydraulic conditions varied in wave height and period (Table 2), while the water depth at the toe of the beach was kept constant (h = 0.4 m). The (offshore) wave steepness ($H_s/L_{p,o}$) varied from about 0.015 to 0.028 (Table 2), resulting in relatively low surf similarity parameter values (ξ = 0.28–0.39), suggesting spilling as the dominant breaking type [*Battjes*, 1974].

For all seven irregular wave experiments, model simulations are run for 100·T_p seconds in both nonhydrostatic and surfbeat mode after a 300 s spin-up period. First-order wave steering is applied, hence IG motions are only generated within the flume itself and not at the boundary, which is consistent with the flume experiments. The vegetation is included using the parameters (i.e., vegetation stem diameter, density, and height) described earlier. The (bulk) drag coefficient is estimated as function of the Keulegan-Carpenter number using a relation for rigid vegetation derived by *Ozeren et al.* [2014]. Since the resulting C_D-values are all close to 1.7 (1.64–1.74), a constant bulk drag coefficient of 1.7 is used for all simulations. For all other model settings, default values are used.

First, the results for case r40091240, which are representative for the other cases, are discussed individually. Without vegetation, the measured total wave height shows a characteristic cross-shore development with first wave shoaling and subsequently energy dissipation due to breaking when the local water depth decreases (Figure 3a). The measured mean water level (Figure 3e) shows a relatively noisy signal in cross-shore direction (mainly between x = 8 and x = 14 m). It slightly decreases in the shoaling zone, and subsequently strongly increases in the breaker zone due to the wave setup. In case of vegetation, wave energy is dissipated by the vegetation stems before the break point is reached, resulting in much lower wave heights at relatively deep water (Figure 3a), similar to the results of *Løvås* [2000]. More interesting is the effect of vegetation on the mean water level. In case of vegetation, the mean water level nearshore is much lower than in case of no vegetation (Figure 3e).

The total significant wave height (Figures 3a and 3b), infragravity wave height (Figures 3c and 3d), and mean water level (Figures 3e and 3f) are computed with nonhydrostatic (Figures 3a, 3c, and 3e) and surfbeat mode (Figures 3b, 3d, and 3f) for run r40091240 with and without vegetation. In case of no vegetation, the total wave height is somewhat overestimated in the surf zone, mainly for surfbeat mode (bias = 0.26 cm, SCI = 0.10), though the location of wave breaking is accurately reproduced in both modes. The mean water level shows a typical set-down (shoaling zone) and setup (breaker and surf zone) development. The nearshore mean water level is underpredicted, which is related to overestimation of the sea-swell wave height (Figures 3a and 3b).

In case of vegetation, excellent results are obtained for the total wave height along the cross-shore profile using both model modes (Figures 3a and 3b): bias = −0.07 cm, SCI = 0.07 (surfbeat) and bias = 0.17 cm, SCI = 0.05 (nonhydrostatic) for all cases combined. For the IG waves (Figures 3c and 3d), both surfbeat and nonhydrostatic show a clear effect of the vegetation, contrary to the findings from the Løvås-experiments (section 4.1). Here the vegetation is responsible for a reduction of the peak IG wave height of more than 50%, which is found consistently for the other six cases (not shown). These results suggest that the vegetation is able to effectively attenuate IG waves, which is likely due to the relatively high vegetation height over water depth ratio, in combination with relatively large drag (combination of vegetation characteristics and drag coefficient) compared to the Løvås-experiments. Unfortunately, these findings could not be verified with the data, as only total wave heights are processed. In nonhydrostatic mode, XBeach is able to accurately capture the effect of vegetation on the mean water level (Figures 3e and 3f). This effect is related to the nonlinear wave shape, and the vegetation being emergent (section 2) which is implicitly taken into account when using the nonhydrostatic mode. In surfbeat mode, however, the wave setup is overpredicted when the net vegetation force is taken as zero (i.e., including the effect of vegetation on the radiation stress force and bed shear stress, but excluding the effect of emergent vegetation and nonlinear waves; Figure 3f). When including the wave shape model to determine the effect of nonlinear waves and emergent vegetation, a much better prediction of the nearshore mean water level is obtained (Figure 3f). The results suggest that nonlinear wave processes are important for the nearshore mean water levels, which is consistent with the theory by *Dean and Bender* [2006].

A comparison is made between measured and computed total significant wave height and mean water level using the nonhydrostatic and surfbeat mode for all seven experiments (as presented in Table 2, see Figure 4). Both the nonhydrostatic (Figure 4a) and surfbeat mode (Figure 4b) accurately reproduce (low bias and scatter index) the total significant wave height both without and with vegetation. Both modes compute the mean water level reasonably well at most locations (Figures 4c and 4d), although the bias in case of no vegetation is relatively high (−0.279 and −0.510 mm, respectively). This is related to the underprediction of the mean water level at very shallow water, which is found throughout the runs (see also Figure 3). For the case with vegetation, the nonhydrostatic mode predicts the mean water level accurately (Figure 4c). Using surfbeat mode, without using the wave shape model, the mean water level is strongly overpredicted (Figure 4d, orange dots). However, when using the wave shape model to account for nonlinear wave effects, the model error is greatly reduced, and the surfbeat mode is able to accurately reproduce the measured water levels (Figure 4d, blue dots). Given the complexity of measuring water levels within the vegetation patch at such small scale and low water depths, it is unclear how suitable these observations are to actually quantify model results, and how the values obtained relate to the measurement accuracy. However, the observations do provide sufficient information for a proper qualitative comparison, since the effect of vegetation on the mean water level is clearly represented (Figure 3).

The results confirm that the model can reproduce the observations of lower wave setup due to vegetation (Figures 3 and 4). The XBeach nonhydrostatic mode is able to directly capture this effect since it resolves the water motions up to the sea-swell wave time scale. However, the XBeach surfbeat mode does not resolve the wave phase, and therefore the wave shape model is needed to accurately predict nearshore mean water levels.

4.3. Importance of the Effect of Vegetation on Wave Setup

At present, limited observations are available on the importance of the effect of vegetation on wave setup. Both *Ma et al*. [2013] and *Guannel et al*. [2015] identified the effect from variations in their model configurations but these were not supported by data. Although the laboratory data obtained by *Wu et al*. [2011] has been invaluable for this work, the experiments were performed using identical experimental configurations (i.e., constant bed profile and vegetation lay-out). The authors are not aware of any other laboratory or field study that could confirm the process. It is therefore difficult to determine the importance of the effect of vegetation on wave setup in practical applications with natural vegetation.

To study the potential importance of vegetation processes on wave setup on different coastal geomorphological configurations, a series of model runs is set up using case r40091240 of the experiments by *Wu et al*. [2011] as reference. With the wave conditions and vegetation characteristics kept constant, the bed profile is varied from 1/10, 1/20, 1/50, 1/100, 1/200 to 1/500, representing relatively steep-sloping to mild-sloping

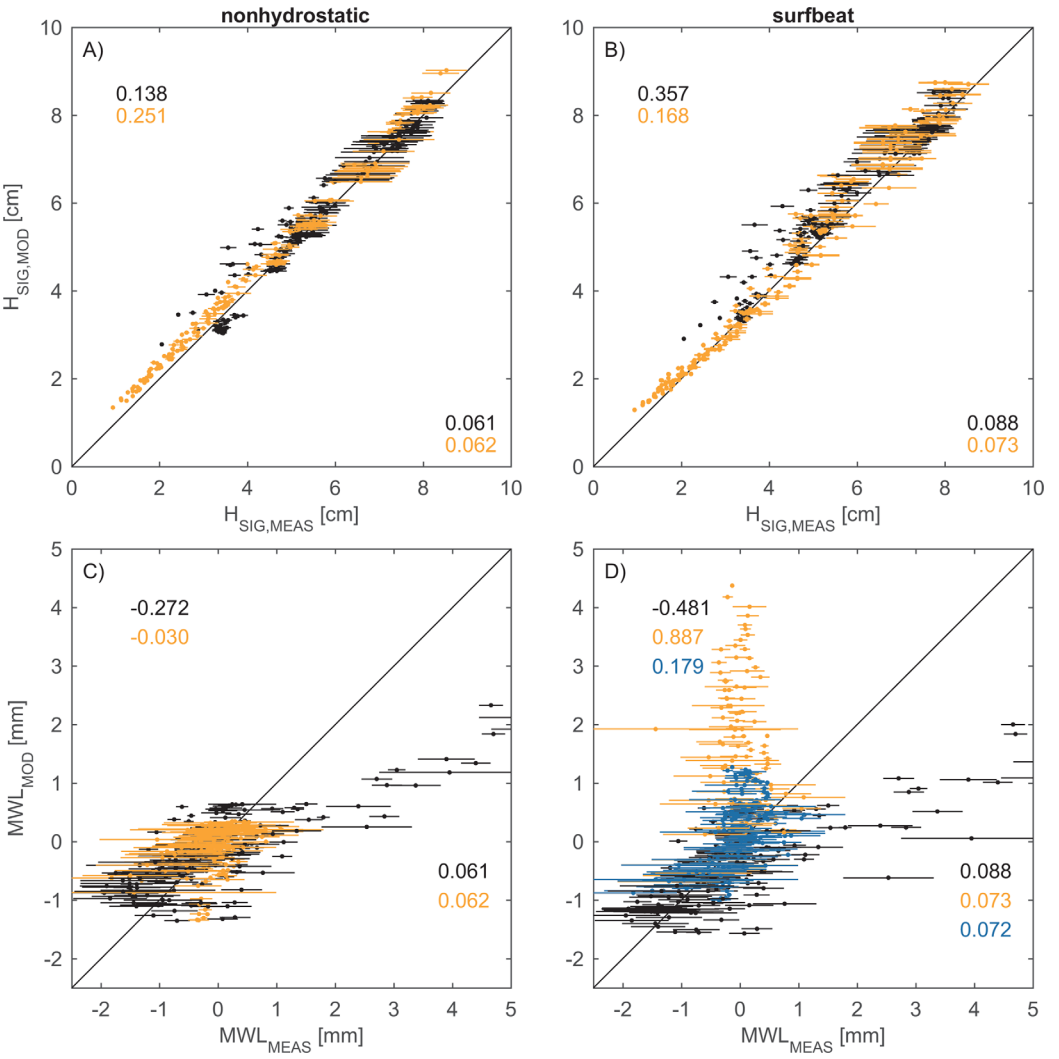

Figure 4. Comparison of measured (horizontal) and computed (vertical) (a, b) total significant wave height and (c, d) mean water level for seven irregular wave flume experiments with and without vegetation by *Wu et al.* [2011], see Table 2. Mean values obtained from repeating the experiments are indicated with black (no vegetation) or colored (with vegetation) dots. Horizontal lines indicate the spreading in obtained values (mean plus and minus one standard deviation of the measurements). The surfbeat mode was run with (blue) and without (orange) (d) nonlinear wave effects. Model skill is computed using bias (top left) and scatter index (bottom right).

coasts. In addition, the offshore extent of the vegetation field is varied as function of the local still water depth, and the incident offshore wave height: $h_{veg,offshore}$ = 1, 2, 3, 4, and 5 times $H_{m0,offshore}$ (= 6.7 cm, see Table 2). These variations (including no vegetation) result in 36 model cases, which are run using surfbeat mode with and without the wave shape model. For verification, all model cases are also run in nonhydrostatic mode.

The resulting wave setup at the still water line is computed for all simulations (Figure 5). The results using nonhydrostatic mode (Figure 5a) show that the computed wave setup is positively correlated with the beach slope, which is consistent with many previous studies and with commonly used empirical relations [e.g., *Stockdon et al.*, 2006]. Furthermore, the wave setup reduces more when the vegetation field extents further offshore. In the case of typical sandy coastal slopes (1/10 and 1/20), the wave setup gradually decreases to zero or even becomes slightly negative (set-down, not shown here). For gentler slopes, the wave setup reduces relatively fast, independent of the extent of the vegetation. Note that in the cases with a relatively gentle slope, the horizontal extent of the vegetation field is much larger than for the relatively steep slopes for the same water depth.

Similar trends are computed using the surfbeat mode (Figure 5b) compared to the nonhydrostatic mode, however, some differences can be found in individual model runs. For instance, the wave setup in the

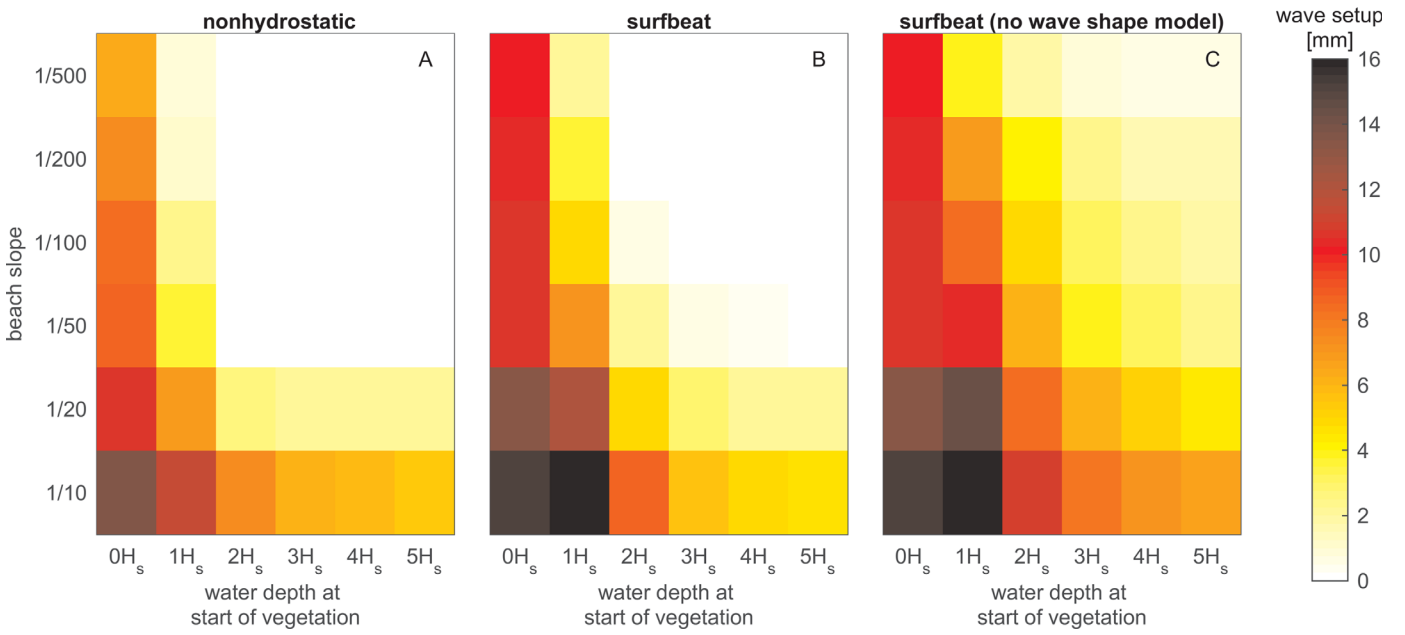

Figure 5. Wave setup at the still water line as computed by XBeach in (a) nonhydrostatic mode, (b) surfbeat mode with wave shape model, and (c) surfbeat without wave shape model for a range of variations in beach slope (1/10–1/500, vertical axis) and still water depth at the start of the vegetation field (as function of the offshore significant wave height, horizontal axis, note that $0{\cdot}H_s$ represents no vegetation).

absence of vegetation is generally overestimated. Both the nonhydrostatic and surfbeat mode show a relatively strong reduction in wave setup, particularly in case of vegetation being present at relatively deep water ($h_{veg,offshore} > 2{\cdot}H_{m0,offshore}$).

When the wave shape model is not taken into account (Figure 5c), the wave setup is relatively high for all cases. The setup in these simulations does decrease as a function of the offshore extent of the vegetation field, which can be attributed to the combined radiation stress gradient and bed shear stress effects (section 2). However, when considering the nonhydrostatic mode as a reference, it is clear that the wave shape effect has a large contribution. These modeling results indicate that taking intrawave vegetation interaction processes into account (either directly or through approximations) in determining nearshore water levels may be important for a range of coastal geomorphological configurations.

5. Discussion

5.1. Applicability of Results for Real-World Situations

In the previous section, the model was verified using two laboratory experiments that used mimic vegetation. Recently, several researchers have used live vegetation in wave flume studies [e.g., *Möller et al.*, 2014; *Maza et al.*, 2015], providing a more accurate representation of the effect of vegetation on the local hydrodynamics. The main advantage of using real vegetation in a wave flume over conducting field experiments is the ability to control the hydrodynamic conditions that the plants are subject to. However, to our knowledge, the effect of vegetation on wave setup has not been measured yet in laboratory studies using real vegetation nor the in the field, hence such data could not be used in the current study.

In case of mimic vegetation in flume studies, some authors choose to use rigid cylinders [e.g., *Akgul et al.*, 2013; *Hu et al.*, 2014], while others opt for flexible mimics [e.g., *Løvås*, 2000; *Luhar et al.*, 2010]. In both cases, the effect of mimic vegetation on the local hydrodynamics provides a more simplified version of reality than real vegetation. Here model formulations that are based on a rigid-cylinder concept are developed and applied to two different data sets in which both flexible (section 4.1) and rigid (section 4.2) mimic vegetation was used. We found that the model is able to reproduce the observations well in both cases. Even though vegetation may be often much more complicated in natural settings (e.g., vertical, spatial, and/or seasonal variation in vegetation properties), the results indicate that the model captures the essential

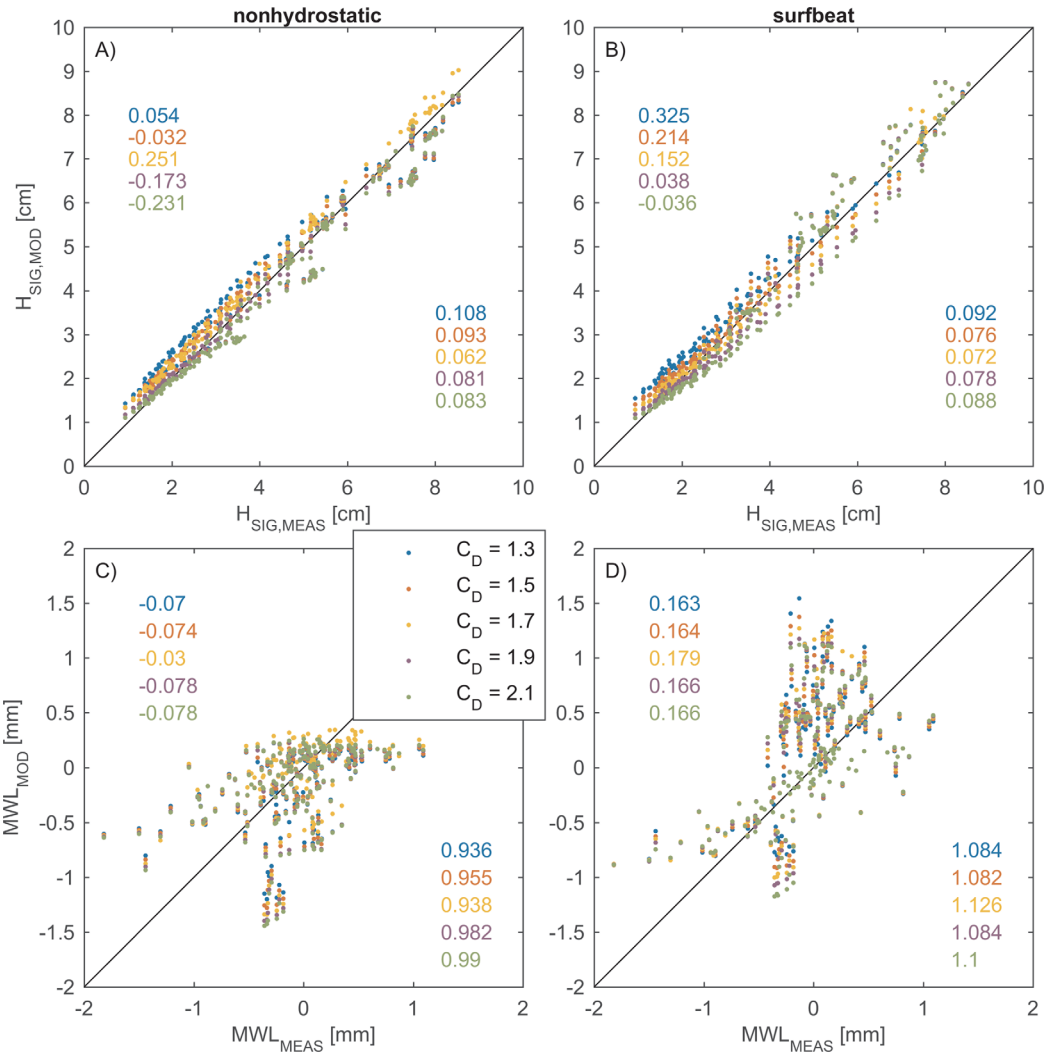

Figure 6. Comparison of measured (horizontal) and computed (vertical) (a, b) total significant wave height and (c, d) mean water level for seven irregular wave flume experiments by *Wu et al.* [2011] with vegetation, using five different (constant) values for the drag coefficient (C_D). The model skill is represented by the bias (top left) and scatter index (bottom right) in each plot.

physical processes (i.e., effect on sea-swell wave, IG waves and wave setup). Although the rigid-cylinder concept used here is not strictly valid for flexible vegetation (e.g., seagrass), it is expected that the major part of uncertainty in real-world situations will result from the estimation of (spatially and seasonally varying) vegetation characteristics.

The results furthermore provide a first indication on the importance of the effect of aquatic vegetation on wave setup, and suggest that this effect may play a role on different typical (vegetated) coastal geomorphological configurations (i.e., on relatively steep to gentle slope coasts with varying vegetation extents). However, as mentioned earlier, this could not be verified here using any (full-scale) field data. Wave setup is directly correlated to the incident wave energy, and the effect of vegetation on wave setup is therefore expected to be most relevant during high-energy (storm) conditions. Therefore, the next step would be to measure this effect under storm conditions either in the field on in a large-scale research facility [e.g., *Möller et al.*, 2014]. These measurements could then be used to confirm our findings and further validate our modeling methodology for naturally vegetated coastal environments.

5.2. Choice of Drag Coefficient

A notable difference between the current and several other studies is the use of a constant (bulk) drag coefficient, rather than a time-varying drag coefficient related to the local Keulegan-Carpenter number (*KC*) or

Reynolds number. Over the past years, authors have used several methods to determine realistic C_D-values. For instance, *Mendez and Losada* [2004] used the experiments by *Dubi* [1995] to relate the bulk drag coefficient in their formulation to *KC*. Since then, several authors adopted their relation in their own models [e.g., *Li and Zhang*, 2010; *Ma et al*., 2013]. *Ozeren et al*. [2014] used a similar approach for a range of different cases varying in vegetation type (rigid versus flexible, artificial versus real) and wave conditions (regular and irregular waves), and derived different drag coefficient relations as a function of *KC*. Although the drag coefficient shows a clear relation with *KC*, the relation varies significantly among different vegetation types or species [e.g., *Ozeren et al*. 2014]. Novel measurement techniques allow for a more accurate determination of the drag coefficient. For instance, *Hu et al*. [2014] quantified the drag coefficient by a direct force measurement technique in a wave flume. They used data from a force transducer in the flume bed that was attached to a number of rigid vegetation stems in combination with velocity profile measurements. Using the Morison equation [*Morison et al*., 1950, equation (1)], they were able to directly compute C_D. However, for practical applications, it is often challenging to determine the physical characteristics (e.g., height and density) of vegetation, since they vary strongly among different species and are often subject to seasonal changes [e.g., *Möller and Spencer*, 2002; *Paul and Amos*, 2011]. The (bulk) drag coefficient is even more difficult to determine, and therefore often values from literature (e.g., laboratory experiments) are used in practical applications.

In this study, a constant bulk drag coefficient was estimated based on empirical relations found in literature. To investigate the model sensitivity to the C_D-value, the experimental cases of *Wu et al*. [2011] are rerun for a range of C_D-values (1.3–2.1) with steps of 0.2. Both the nonhydrostatic and surfbeat mode show a relatively minor effect of C_D in the modeled wave heights and mean water levels (Figure 6). Relatively good results can be obtained with the model, even in the case of limited information on the vegetation where a drag coefficient needs to be estimated. The relatively low sensitivity of the results to the choice of drag coefficient is encouraging for practical engineering applications (e.g., storm impact studies), where accurate data on vegetation characteristics are often lacking. Note that here the model was applied to cases with $KC > 10$ only. In case of relatively low *KC*, the bulk drag coefficient generally increases rapidly with decreasing *KC* [e.g., *Ozeren et al*., 2014]. As a universal description of the bulk drag coefficient in oscillatory flow is currently lacking, it is important to choose an appropriate empirical relation from literature, particularly for cases with relatively low *KC*.

5.3. Validity of the Wave Shape Model for Vegetated Coasts

The wave shape model employed within this study is based on the empirical formulation by *Ruessink et al*. [2012], which was derived from a large data set (30,000+ field observations) of wave skewness and asymmetry, using data from coasts without vegetation. Although our understanding of the effect of vegetation on the wave shape is currently lacking, the results of *Wu et al*. [2011] suggest that vegetation mainly affects wave asymmetry rather than skewness. Since wave asymmetry does not contribute to the net force that affects the wave setup, and the results of the current study show that the surfbeat approach with wave shape model produces similar results as the intrawave nonhydrostatic mode, it is assumed that the effect of vegetation on the wave shape is limited, and the wave shape model is therefore able to accurately capture the intrawave vegetation effects described in section 2.

6. Conclusions

This paper presents formulations that describe the attenuation of sea-swell and infragravity wave energy and wave setup on coasts fronted by vegetation. The formulations are implemented in the open-source XBeach model, in two modes. Both the nonhydrostatic (phase-resolving) and surfbeat (phase-averaged) mode are verified for sea-swell and IG wave heights as well as mean water level (MWL) or wave setup using data from two laboratory experiments with mimic vegetation. The wave-vegetation interaction on the intrawave scale (i.e., in case of emergent vegetation and/or nonlinear waves) is found to be important, and should be included to obtain accurate predictions of the nearshore MWL. In nonhydrostatic mode, these effects are directly simulated and the model-data agreement is generally good. In the surfbeat mode, a wave shape model is implemented to estimate the wave phase. Without using the wave shape model, the nearshore MWL is strongly overpredicted, which may potentially lead to a general overestimation of coastal hazards in storm impact studies and underestimation of the coastal protection service provided by vegetation.

Subsequently, the model is used to study the importance of the effect of vegetation on wave setup. Model results indicate this effect may be relevant on a range of coastal geomorphological configurations with varying bed slopes and vegetation extents. Further measurements of wave setup in naturally vegetated environments are required to confirm this hypothesis.

Appendix A: Description of Wave Shape Model

The wave shape model employed within this paper is similar to the model presented by *van Thiel de Vries* [2009]. It utilizes the parameterization by *Rienecker and Fenton* [1981], in which the sea-swell wave shape is described by the weighted sum of eight sine and cosine functions:

$$u_w = \sum_{i=1}^{i=8} wA_i \cos(i\omega t) + (1-w)A_i \sin(i\omega t) \tag{A1}$$

where u_w is the sea-swell wave velocity, A_i is the amplitude of a specific harmonic i, ω is the angular wave frequency, and w is a weighting function. The weight function is calculated as function of the phase φ, which is estimated using an empirical formulation [*Ruessink et al*., 2012]:

$$\begin{aligned} w &= 1-\varphi/\pi \\ \varphi &= \frac{\pi}{2}\left(1-\tanh\left(\frac{0.815}{U_r^{0.672}}\right)\right) \end{aligned} \tag{A2}$$

where the Ursell number (U_r) is given by:

$$U_r = \frac{3}{8}\frac{Hk}{(kh)^3} \tag{A3}$$

Using stream function theory [*Rienecker and Fenton*, 1981], near-bed velocity amplitudes (A_i) are computed for a wide range of wave conditions, and tabulated based on nondimensional wave height and nondimensional wave period. Given the local wave height, wave period, and water depth, the velocity amplitude is found in the table and a velocity time series can be obtained.

Acknowledgments

This work was funded through the Office of Naval Research Coastal Geosciences Program "Modeling the Mekong Delta at three different scales" (grant N00014-12-1-0433), and through the "Hydro- and morphodynamics during extreme events" research program (1230002) funded by Deltares. The authors would like to thank Yavuz Ozeren, Stig Magnar Løvås, and Øivind Arntsen for providing the laboratory data used in this study, as well as an anonymous reviewer who helped to improve this manuscript. The extended code developed within this study is part of the open-source XBeach code and can be downloaded at www.xbeach.org. The profile models can be obtained by sending a written request to the corresponding author at arnold.vanrooijen@deltares.nl.

References

Abdelrhman, M. A. (2007), Modeling coupling between eelgrass Zostera marina and water flow, *Mar. Ecol. Progress Ser.*, *338*, 81–96, doi:10.3354/meps338081.

Akgul, M. A., D. Yilmazer, E. Oguz, M. S. Kabdasli, and O. Yagci (2013), The effect of an emergent vegetation (i.e. Phragmistes Australis) on wave attenuation and wave kinematics, *J. Coastal Res.*, *1*, 147–152, doi:10.2112/SI65-026.1.

Apotsos, A., B. Raubenheimer, S. Elgar, R. T. Guza, and J. A. Smith (2007), Effects of wave rollers and bottom stress on wave setup, *J. Geophys. Res.*, *112*, C02003, doi:10.1029/2006JC003549.

Battjes, J. A. (1974), Computation of set-up, longshore currents, run-up and overtopping due to wind-generated waves, PhD thesis, Fac. of Civ. Eng. and Geosci., Delft Univ. of Technol., Delft, Netherlands.

Borsje, B. W., B. K. van Wesenbeeck, F. Dekker, P. Paalvast, T. J. Bouma, M. M. van Katwijk, and M. B. de Vries (2011), How ecological engineering can serve in coastal protection, *Ecol. Eng.*, *37*(2), 113–122, doi:10.1016/j.ecoleng.2010.11.027.

Buckley, M. L., R. J. Lowe, J. E. Hansen, and A. R. van Dongeren (2016), Wave setup over a fringing reef with large bottom roughness, *J. Phys. Oceanogr.*, doi:10.1175/JPO-D-15-0148.1, in press.

Dalrymple, R. A., J. T. Kirby, and P. A. Hwang (1984), Wave diffraction due to areas of energy dissipation, *J. Waterw. Port Coastal Ocean Eng.*, *110*(1), 67–79, doi:10.1061/(ASCE)0733-950X(1984)110:1(67).

Dean, R. G., and C. J. Bender (2006), Static wave setup with emphasis on damping effects by vegetation and bottom friction, *Coastal Eng.*, *53*(2), 149–156, doi:10.1016/j.coastaleng.2005.10.005.

Dijkstra, J. T., and R. E. Uittenbogaard (2010), Modeling the interaction between flow and highly flexible aquatic vegetation, *Water Resour. Res.*, *46*, W12547, doi:10.1029/2010WR009246.

Döbken, J. W. (2015), Modeling the interaction between wave hydrodynamics and flexible aquatic vegetation, MSc thesis, Fac. of Civ. Eng. and Geosci., Delft Univ. of Technol., Delft, Netherlands.

Dubi, A. M. (1995), Damping of water waves by submerged vegetation: A case study on Laminaria hyperborea, PhD thesis, Dep. Of Struct. Eng., The Norw. Inst. of Technol., Univ. of Trondheim, Trondheim, Norway.

Guannel, G., P. Ruggiero, J. Faries, K. Arkema, M. Pinsky, G. Gelfenbaum, A. Guerry, and C.-K. Kim (2015), Integrated modeling framework to quantify the coastal protection services supplied by vegetation, *J. Geophys. Res. Oceans*, *120*, 324–345, doi:10.1002/2014JC009821.

Horstman, E. M., C. M. Dohmen-Janssen, P. M. F. Narra, N. J. F. van den Berg, M. Siemerink, and S. J. M. H. Hulscher (2014), Wave attenuation in mangroves: A quantitative approach to field observations, *Coastal Eng.*, *94*, 47–62, doi:10.1016/j.coastaleng.2014.08.005.

Hu, Z., T. Suzuki, T. Zitman, W. Uittewaal, and M. Stive (2014), Laboratory study on wave dissipation by vegetation in combined current–wave flow, *Coastal Eng.*, *88*, 131–142, doi:10.1016/j.coastaleng.2014.02.009.

Kobayashi, N., A. W. Raichle, and T. Asano (1993), Wave attenuation by vegetation, *J. Waterw. Port Coastal Ocean Eng.*, *119*(1), 30–48, doi:10.1061/(ASCE)0733-950X(1993)119:1(30).

Koch, E., et al. (2009), Non-linearity in ecosystem services: Temporal and spatial variability in coastal protection, *Frontiers Ecol. Environ.*, *7*(1), 29–37, doi:10.1890/080126.
Li, C. W., and M. L. Zhang (2010), 3D modelling of hydrodynamics and mixing in a vegetation field under waves, *Comput. Fluids*, *39*(4), 604–614, doi:10.1016/j.compfluid.2009.10.010.
Longuet-Higgins, M. S., and R. W. Stewart (1964), Radiation stresses in water waves: A physical discussion, with applications, *Deep Sea Res. Oceanogr. Abstr.*, *11*(4), 529–562, doi:10.1016/0011-7471(64)90001-4.
Løvås, S. M. (2000), Hydro-physical conditions in kelp forests and the effect on wave damping and dune erosion: A case study on Laminaria hyperborea, PhD thesis, Fac. of Civ. and Environ. Eng., Norw. Univ. of Sci. and Technol., Trondheim, Norway.
Løvås, S. M., and A. Tørum (2001), Effect of the kelp Laminaria hyperborea upon sand dune erosion and water particle velocities, *Coastal Eng.*, *44*(1), 37–63, doi:10.1016/S0378-3839(01)00021-7.
Lövstedt, C. B., and M. Larson (2010), Wave damping in reed: Field measurements and mathematical modeling, *J. Hydrol. Eng.*, *136*(4), 222–233, doi:10.1061/(ASCE)HY.1943-7900.0000167.
Luhar, M., S. Coutu, E. Infantes, S. Fox, and H. Nepf (2010), Wave-induced velocities inside a model sea grass bed, *J. Geophys. Res.*, *115*, C12005, doi:10.1029/2010JC006345.
Ma, G., J. T. Kirby, S. F. Su, J. Figlusand, and F. Shi (2013), Numerical study of turbulence and wave damping induced by vegetation canopies, *Coastal Eng.*, *80*, 68–78, doi:10.1016/j.coastaleng.2013.05.007.
Maza, M., J. L. Lara, I. J. Losada, B. Ondiviela, J. Trinogga, and T. J. Bouma (2015), Large-scale 3-D experiments of wave and current interaction with real vegetation. Part 2: Experimental analysis, *Coastal Eng.*, *106*, 73–86, doi:10.1016/j.coastaleng.2015.09.010.
Mazda, Y., M. Magi, M. Kogo, and P. N. Hong (1997), Mangroves as a coastal protection from waves in the Tong King delta, Vietnam, *Mangroves Salt Marshes*, *1*(2), 127–135, doi:10.1023/A:1009928003700.
McCall, R. T., J. van Thiel De Vries, N. G. Plant, A. R. van Dongeren, J. A. Roelvink, D. M. Thompson, and A. J. H. M. Reniers (2010), Two-dimensional time dependent hurricane overwash and erosion modeling at Santa Rosa Island, *Coastal Eng.*, *57*(7), 668–683, doi:10.1016/j.coastaleng.2010.02.006.
McCall, R. T., G. Masselink, T. G. Poate, J. A. Roelvink, L. P. Almeida, M. Davidson, and P. E. Russell (2014), Modelling storm hydrodynamics on gravel beaches with XBeach-G, *Coastal Eng.*, *91*, 231–250, doi:10.1016/j.coastaleng.2014.06.007.
Mendez, F. J., and I. J. Losada (2004), An empirical model to estimate the propagation of random breaking and nonbreaking waves over vegetation fields, *Coastal Eng.*, *51*(2), 103–118, doi:10.1016/j.coastaleng.2003.11.003.
Möller, I., and T. Spencer (2002), Wave dissipation over macro-tidal saltmarshes: Effects of marsh edge typology and vegetation change, *J. Coastal Res.*, *36*(1), 506–521.
Möller, I., et al. (2014), Wave attenuation over coastal salt marshes under storm surge conditions, *Nat. Geosci.*, *7*(10), 727–731, doi:10.1038/ngeo2251.
Morison, J. R., J. W. Johnson, and S. A. Schaaf (1950), The force exerted by surface waves on piles, *J. Pet. Technol.*, *2*(05), 149–154, doi:10.2118/950149-G.
Mullarney, J. C., and S. M. Henderson (2010), Wave-forced motion of submerged single-stem vegetation, *J. Geophys. Res.*, *115*, C12061, doi:10.1029/2010JC006448.
Ozeren, Y., D. G. Wren, and W. Wu (2014), Experimental investigation of wave attenuation through model and live vegetation, *J. Waterw. Port Coastal Ocean Eng.*, *140*(5), 04014019-1–04014019-12, doi:10.1061/(ASCE)WW.1943-5460.0000251.
Paul, M., and C. L. Amos (2011), Spatial and seasonal variation in wave attenuation over Zostera noltii, *J. Geophys. Res.*, *116*, C08019, doi:10.1029/2010JC006797.
Phan, L. K., J. S. M. van Thiel de Vries, and M. J. F. Stive (2015), Coastal Mangrove Squeeze in the Mekong Delta, *J. Coastal Res.*, *31*(2), 233–243, doi:10.2112/JCOASTRES-D-14-00049.1.
Phillips, O. M. (1977), *The Dynamics of the Upper Ocean*, 2nd ed., 336 pp., Cambridge Univ. Press, Cambridge, U. K.
Quartel, S., A. Kroon, P. G. E. F. Augustinus, P. van Santen, and N. H. Tri (2007), Wave attenuation in coastal mangroves in the Red River Delta, Vietnam, *J. Asian Earth Sci.*, *29*(4), 576–584, doi:10.1016/j.jseaes.2006.05.008.
Quataert, E., C. Storlazzi, A. van Rooijen, O. Cheriton, and A. van Dongeren (2015), The influence of coral reefs and climate change on wave-driven flooding of tropical coastlines, *Geophys. Res. Lett.*, *42*, 6407–6415, doi:10.1002/2015GL064861.
Reniers, A. J. H. M., J. A. Roelvink, and E. B. Thornton (2004), Morphodynamic modeling of an embayed beach under wave group forcing, *J. Geophys. Res.*, *109*, C01030, doi:10.1029/2002JC001586.
Rienecker, M. M., and J. D. Fenton (1981), A Fourier approximation method for steady water waves, *J. Fluid Mech.*, *104*, 119–137, doi:10.1017/S0022112081002851.
Roelvink, D., A. Reniers, A. van Dongeren, J. van Thiel de Vries, R. McCall, and J. Lescinski (2009), Modelling storm impacts on beaches, dunes and barrier islands, *Coastal Eng.*, *56*(11), 1133–1152, doi:10.1016/j.coastaleng.2009.08.006.
Roelvink, J. A. (1993), Dissipation in random wave groups incident on a beach, *Coastal Eng.*, *19*(1), 127–150, doi:10.1016/0378-3839(93)90021-Y.
Ruessink, B. G., J. R. Miles, F. Feddersen, R. T. Guza, and S. Elgar (2001), Modeling the alongshore current on barred beaches, *J. Geophys. Res.*, *106*(C10), 22,451–22,463, doi:10.1029/2000JC000766.
Ruessink, B. G., G. Ramaekers, and L. C. van Rijn (2012), On the parameterization of the free-stream non-linear wave orbital motion in near-shore morphodynamic models, *Coastal Eng.*, *65*, 56–63, doi:10.1016/j.coastaleng.2012.03.006.
Ruggiero, P., P. D. Komar, W. G. McDougal, J. J. Marra, and R. A. Beach (2001), Wave runup, extreme water levels and the erosion of properties backing beaches, *J. Coastal Res.*, *17*(2), 407–419.
Smit, P., M. Zijlema, and G. Stelling (2013), Depth-induced wave breaking in a non-hydrostatic, near-shore wave model, *Coastal Eng.*, *76*, 1–16, doi:10.1016/j.coastaleng.2013.01.008.
Smit, P. B., G. S. Stelling, J. A. Roelvink, J. van Thiel de Vries, R. T. McCall, A. R. van Dongeren, C. Zwinkels, and R. Jacobs (2010), XBeach: Non-hydrostatic model: Validation, verification and model description, technical report, Delft Univ. of Technol., Delft, Netherlands.
Stelling, G., and M. Zijlema (2003), An accurate and efficient finite-difference algorithm for non-hydrostatic free-surface flow with application to wave propagation, *Int. J. Numer. Methods in Fluids*, *43*(1), 1–23, doi:10.1002/fld.595.
Stockdon, H. F., R. A. Holman, P. A. Howd, and A. H. Sallenger (2006), Empirical parameterization of setup, swash, and runup, *Coastal Eng.*, *53*(7), 573–588, doi:10.1016/j.coastaleng.2005.12.005.
Stratigaki, V., E. Manca, P. Prinos, I. J. Losada, J. L. Lara, M. Sclavo, C. L. Amos, I. Caceres, and A. Sánchez-Arcilla (2011), Large-scale experiments on wave propagation over Posidonia oceánica, *J. Hydrol. Res.*, *49*, suppl. 1, 31–43, doi:10.1080/00221686.2011.583388.
Suzuki, T., M. Zijlema, B. Burger, M. C. Meijer, and S. Narayan (2012), Wave dissipation by vegetation with layer schematization in SWAN, *Coastal Eng.*, *59*(1), 64–71, doi:10.1016/j.coastaleng.2011.07.006.

Svendsen, I. A. (2006), *Introduction to Nearshore Hydrodynamics, Adv. Ser. Ocean Eng.*, vol. 24, 744 pp., World Sci., Singapore.
Tang, J., S. Shen, and H. Wang (2015), Numerical model for coastal wave propagation through mild slope zone in the presence of rigid vegetation, *Coastal Eng.*, *97*, 53–59, doi:10.1016/j.coastaleng.2014.12.006.
Van der Westhuysen, A. J. (2010), Modeling of depth-induced wave breaking under finite depth wave growth conditions, *J. Geophys. Res.*, *115*, C01008, doi:10.1029/2009JC005433.
Van Dongeren, A., R. Lowe, A. Pomeroy, D. M. Trang, D. Roelvink, G. Symonds, and R. Ranasinghe (2013), Numerical modeling of low-frequency wave dynamics over a fringing coral reef, *Coastal Eng.*, *73*, 178–190, doi:10.1016/j.coastaleng.2012.11.004.
Van Thiel de Vries, J. S. M. (2009), Dune erosion during storm surges, PhD thesis, Fac. of Civ. Eng. and Geosci., Delft Univ. of Technol., Delft, Netherlands.
Wei, Z., and Y. Jia (2014), Simulation of nearshore wave processes by a depth-integrated non-hydrostatic finite element model, *Coastal Eng.*, *83*, 93–107, doi:10.1016/j.coastaleng.2013.10.002.
Wu, W., et al. (2011), Phase I Report for SERRI Project No. 80037: Investigation of surge and wave reduction by vegetation, report, *Lab. Publ. 1*, 315 pp., SERRI Report 80037-01, Oak Ridge National Laboratory, Oak Ridge, Tenn.
Zhou, C. Y., and J. M. R. Graham (2000), A numerical study of cylinders in waves and currents, *J. Fluids Struct.*, *14*(3), 403–428, doi:10.1006/jfls.1999.0276.
Zijlema, M., G. Stelling, and P. Smit (2011), SWASH: An operational public domain code for simulating wave fields and rapidly varied flows in coastal waters, *Coastal Eng.*, *58*(10), 992–1012, doi:10.1016/j.coastaleng.2011.05.015.